JOURNAL OF MATERIALS SCIENCE **39** (2004) 6723–6734

Analytical transmission electron microscopy and surface spectroscopy of ceramics: The microstructural evolution in titanium-doped chromia polycrystals as a function of sintering conditions

S. P. McBRIDE, R. BRYDSON
Institute for Materials Research, University of Leeds, Leeds, LS2 9JT, UK
E-mail: mtlrmdb@leeds.ac.uk

Titanium-doped chromium oxide has been successfully employed in the form of thick film gas sensing devices where the porosity and surface conditioning are key aspects in providing a measurable gas response. Under normal gaseous atmospheres, where the partial oxygen pressure ($p(O_2)$) is approximately 0.2 atm, sintering of the host material (α-Cr_2O_3) to high densities is not possible, instead, significant grain growth occurs through evaporation-condensation transport mechanisms owing to the volatility of non-sesquioxide phases formed at high temperatures. The doping of α-Cr_2O_3 with Ti does not significantly affect the sintering behaviour of the host oxide under atmospheric conditions, but instead tends to form a nanodimensional, surface-segregated ternary phase of a nominal composition: $Cr_2Ti_2O_7$, whilst the composition of grain interiors is close to pure α-Cr_2O_3. By reducing the $p(O_2)$ to $\sim 10^{-15}$ atm during sintering, thereby reducing the formation of volatile phases, solid state diffusion mechanisms have been encouraged allowing the densification of green bodies to a density >99% of the theoretical value. Ceramic bodies obtained by sintering in reduced $p(O_2)$ atmospheres display a single phase solid solution, isostructural with α-Cr_2O_3 (space group R3c). © *2004 Kluwer Academic Publishers*

1. Introduction

This article is designed to highlight the power of analytical transmission electron microscopy (TEM), when combined with other techniques such as surface analysis and diffraction methods, in the detailed study of microstructure-property-processing relationships in complex, commercial ceramic systems. As such it reviews a recent study of the chromia system, in particular the effects of titania doping on the sintering behaviour and resultant chemical and microstructural development in this material. Such effects are of critical importance in determining the overall electrical response of electroceramic devices incorporating doped-chromia thin films.

Chromia, α-Cr_2O_3, possesses the corundum structure with a hexagonal close packed oxygen sub-lattice and it exhibits *p*-type semi-conductivity associated with its oxidative catalytic behaviour in normal gaseous atmospheres. When employed in the form of a thick film, resistive-type gas sensor device [1], the porosity is generally chosen to be approximately 50%, indeed the most gas sensitive structures are only loosely sintered so as to provide a large available surface area for gas adsorption. In the case of chromia, doping with titania, TiO_2, provides a considerably enhanced and controllable response of the oxide to the presence of gaseous phases in the surrounding atmosphere, in particular CO and H_2S. The general mechanism of gas sensing in metal oxide semiconductors relies on the competitive adsorption of oxygen and the particular reducing target gas on the metal oxide ceramic surface and the associated change in conductivity this produces as a function of relative gas partial pressure; interested readers are referred to reference [2] for further information. The detailed mechanisms of gas sensing and the implications of specific microstructural features on sensing properties will not be discussed here, however the phase and microstructural evolution of Ti-doped α-Cr_2O_3 as a function of sintering conditions will be addressed in some detail.

It is reasonably well known that sintering Ti-doped chromia under normal ambient atmospheres leads to the formation of a porous structure which shows porosity levels (which are crucial for highly sensitive gas detection) comparable to that seen in the green compacted structure. Whilst grain growth and particle coarsening can be readily observed during sintering, densification is negligible and surface segregation of Ti is strong. Several studies [3–6] addressing the role of transition metal additives to α-Cr_2O_3 have revealed that solely

Ti assists in the densification of ceramic bodies but only under a reduced partial oxygen pressure, $p(O_2)$, under conditions where the Cr/Cr_2O_3 phase boundary is approached. The most appreciable effect of Ti doping in chromia is a lowering of the sintering temperature from 1600 to 1400°C which can be most satisfactorily explained by the incorporation of Ti^{4+} so modifying the defect structure and raising the diffusivity of rate-controlling migrating species, during thermally activated transport processes. The formation of a liquid phase during sintering has not been observed or predicted and would therefore seem unlikely. The production of non-sesquioxide volatile phases at high temperatures appears to be the main protagonist in the prevention of densification in α-Cr_2O_3. Higher and lower oxides of chromium such as CrO, CrO_2 and Cr_3O_4 are all volatile phases at high temperature and form in significant quantities under normal atmospheres. The evolution of vapour phases controls the sintering behaviour of green bodies and condensation-evaporation transport mechanisms are dominant as the small rounded particles of the green body reduce their surface-derived contribution to their overall free energy. As vapour phase transport is considerable in α-Cr_2O_3 based materials fired in air or in atmospheres containing moderate $p(O_2)$s, grain growth and particle coarsening occurs with almost no measurable change in density from the green state to that seen in fully sintered ceramic compacts.

The characteristics of Ti-doped α-Cr_2O_3 based materials have not been examined extensively in terms of their microstructure and phase evolution as a function of sintering conditions, however surface enrichment of Ti has been reported [7] in porous, device-type materials sintered at moderately high temperatures (~1000°C) in air. As well as characterizing fully the currently available air sintered materials, for comparison, this study also aims to produce highly dense, monolithic ceramics based on the possibility of solid solution formation between titania in α-Cr_2O_3. Such solubility would appear to be a reasonable proposition owing to the fact that the ionic radii of Ti^{4+} and Cr^{3+} are 61 and 60 pm [8] respectively; admittedly other factors such as valency must also be considered but, at low doping levels (<10 at%), the formation of energetically favourable lattice defects should compensate any charge imbalance. Through the use of combined, complementary analytical techniques such as energy filtered transmission electron microscopy (EFTEM) [9], X-ray diffraction (XRD) [10] and X-ray photoelectron spectroscopy (XPS) [11], the structural characteristics and chemical homogeneity of sintered materials have been examined in order to elucidate the microstructural differences between air sintered materials and materials sintered under reducing atmospheres. Such results have also been supported by thermodynamic modelling of the conditions during sintering.

2. Experimental

2.1. Materials preparation

α-Cr_2O_3 (purity >99.2% Elementis Chromium) and TiO_2 (purity >99.9% Cerac Inc) powders (initial particle size 4 and 0.5 μm, respectively as determined by laser diffraction) were milled with alcohol based solvents to obtain a target composition on pre-reaction of $Cr_{1.8}Ti_{0.2}O_{3+x}$ and a particle size 0.5 μm. Both pure chromia and titania-chromia powders were then uniaxially pressed into discs (achieving green densities of approximately 58%) before sintering was performed at a maximum temperature of 1400°C for 4 h. Air fired materials were sintered in α-Al_2O_3 crucibles and exposed to laboratory air during heating. In a separate set of experiments, corresponding samples were also sintered under reducing conditions by forming a ring of activated carbon around the discs thus ensuring that no direct contact between the carbon and ceramic could be made; these samples were also contained in an α-Al_2O_3 crucible which was then fitted with a lid and sealed using a refractory cement (Autostic from Carlton Brown). The activated carbon was present in excess and this removed oxygen from the enclosed atmosphere by forming a CO_2/CO buffer as products in equilibrium. This buffer system was favoured by Ownby and Jungquist [12] who reported the highest sintered densities achieved in the α-Cr_2O_3 system. The consumption of oxygen contained within the crucible volume and also that which may diffuse into the sealed environment at high temperatures, provides control over the formation of undesirable volatile phases and allows the Cr/Cr_2O_3 phase boundary to be approached, which at 1400°C can be calculated to be approximately 5×10^{-15} atm. In such an enclosed system, the relative proportions of solid and vapour phase species may be predicted thermodynamically using, for example, equiTherm (v.3.0) software from VCH Scientific. This method employs a Gibbs energy minimisation procedure to predict the equilibrium state for the system which allows one to follow the evolution of phases as a function of temperature. In the current analysis, the presence of TiO_2 has been omitted as the possible ternary solid phases which may form could not be easily be incorporated into the calculation owing to the absence of reliable thermodynamic data, specifically the enthalpy and entropy of formation, heat capacity and phase transition temperatures of these compounds.

Sintered densities of the fabricated pellets obtained as a function of temperature and atmosphere, were measured using the Archimedes method as detailed in British Standard 7134 Section 1.2: 1989 and are reported for both $Cr_{1.8}Ti_{0.2}O_{3+x}$ and pure α-Cr_2O_3 pellets.

2.2. Materials characterisation

Microstructural analyses of polished and thermally etched sintered samples, were performed using scanning electron microscopy (SEM) (CAMSCAN Series 4). Bulk, phase analysis of pulverised/powdered sintered material was achieved using a Philips APD1700 automated X-ray diffractometer with a monochromated Cu K_α X-ray source. Lattice parameters have been extrapolated from the collected data using a Nelson-Riley refinement for a hexagonal closed packed system.

The surface composition and oxidation state of the cations present in sintered materials has been probed

by XPS, using a VG ESCALAB MK1 instrument with an 300 W Al K_α X-ray source. Samples examined by XPS were not ion beam sputter-cleaned prior to inspection as this can alter the oxidation state of the transition metals present at the surface, especially in the case of Ti containing oxides [13]. Instead, samples were polished to remove the first few microns of material and then ultrasonically cleaned ensuring that any carbon contamination from sintering was removed. All binding energies were charge corrected against the adventitious carbon 1s peak at 285 eV. Elemental quantification of wide scan spectra was undertaken after normalisation of corrected, background-subtracted peak intensities using Wagner sensitivity factors.

TEM analysis was performed with a FEI CM 200 FEGTEM operated at 200 kV and fitted with a Gatan GIF200 electron energy loss spectroscopy (EELS) imaging filter and ultrathin window Oxford Instruments energy dispersive X-ray (EDX) detector. Selected area electron diffraction (SAED) and high resolution phase contrast imaging (HRTEM) were employed to determine lattice structures of crystallites, HRTEM was also used to probe surface structures. Using the GIF, energy filtered images were generated and jump ratio images (two energy window method) at the Ti $L_{2,3}$- and Cr $L_{2,3}$-edges were recorded to observe the microstructural distribution of Ti and Cr. EELS spectra were collected with an energy resolution of 0.8 eV and an energy dispersion of 0.2 eV/channel and quantified for Ti, Cr and O after background subtraction using Hydrogenic cross sections with a correction for the transition metal white line intensities.

3. Results

3.1. Microstructure

The measured densities of both pure α-Cr_2O_3 and $Cr_{1.8}Ti_{0.2}O_{3+x}$ pellets sintered under reducing conditions as a function of temperature are shown in Fig. 1. Densities have been expressed as a percentage of the theoretical density, which for pure α-Cr_2O_3 is 5.21 g cm^{-3} and for $Cr_{1.8}Ti_{0.2}O_{3+x}$ is 5.11 g cm^{-3}; the maximum density attained at 1400°C for these compositions was 93.2% and 99.5% respectively.

As can be seen, densification of Ti-doped α-Cr_2O_3 occurs at significantly lower temperatures than in the undoped material. The exact role of Ti remains unclear, but it would appear that atomic transport mechanisms which lead to densification are enhanced. Both the undoped and doped material have been densified to greater than 90% of the theoretical density under the reducing atmosphere. In comparison, when both compositions were sintered in air, no change in density over the as-pressed state is observed, however considerable grain growth is evident. In Fig. 2, the microstructure of air sintered and reducing atmosphere sintered $Cr_{1.8}Ti_{0.2}O_{3+x}$ materials are compared in SEM secondary electron micrographs.

3.2. Evaluation of sintering atmosphere

At the dwell temperature of 1400°C, equiTherm software was used to calculate the partial pressures of O_2, CO_2 and CO within the sealed crucible and were determined to be 6×10^{-14} atm, 0.11 atm and 21.5 atm respectively. The assumptions made in this calculation were: (i) the contents of the crucible sealed in laboratory air at room temperature did not alter, i.e., the total number of species, either elemental or bound as molecules was constant and (ii) the crucible was inert and played no part in the equilibrium reaction.

3.3. Phase and crystal structure analysis

XRD studies of materials sintered in laboratory air revealed that the undensified material consisted exclusively of two discrete phases, α-Cr_2O_3 and a so-called "E-phase" reportedly of a nominal composition $Cr_2Ti_2O_7$. The E-phase, first reported by Hamelin [14], exists over a wide composition range. The phase diagram for this system [15], for which data has only been

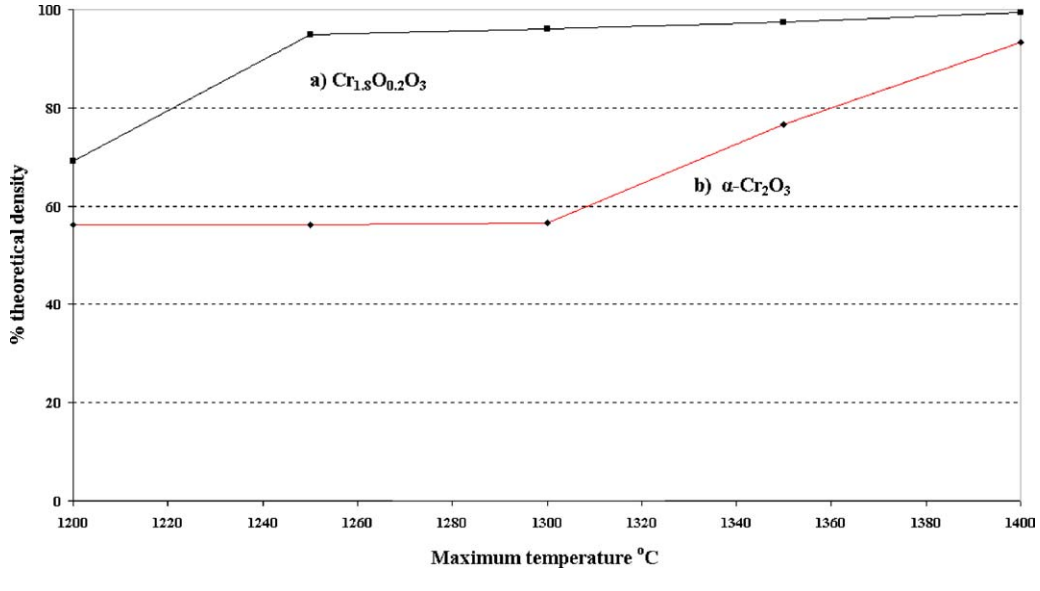

Figure 1 Percentage theoretical density as a function of maximum sintering temperature for: (a) $Cr_{1.8}Ti_{0.2}O_{3+x}$ and (b) α-Cr_2O_3.

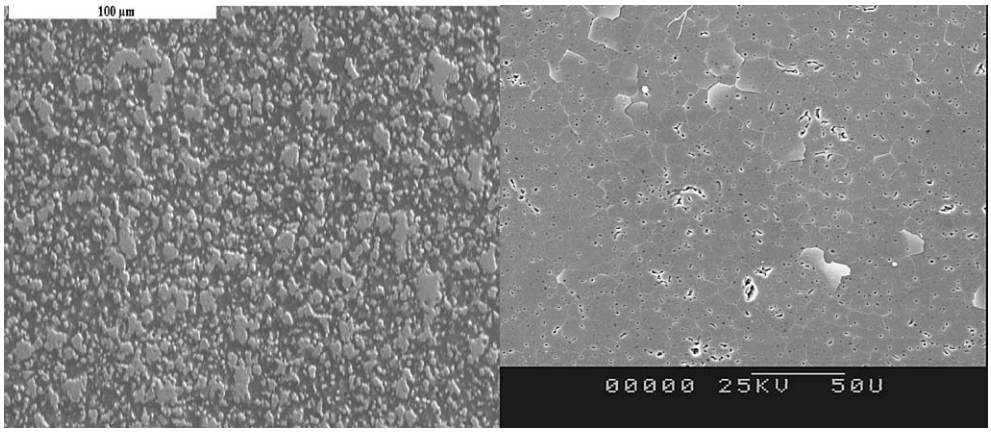

Figure 2 Secondary electron SEM micrographs of: air sintered (left) $Cr_{1.8}Ti_{0.2}O_{3+x}$ exhibiting high levels of porosity and considerable grain growth. (Right) Dense reducing atmosphere sintered $Cr_{1.8}Ti_{0.2}O_{3+x}$, the equiaxed microstructure revealed after thermal etching at 1100°C for 10 min.

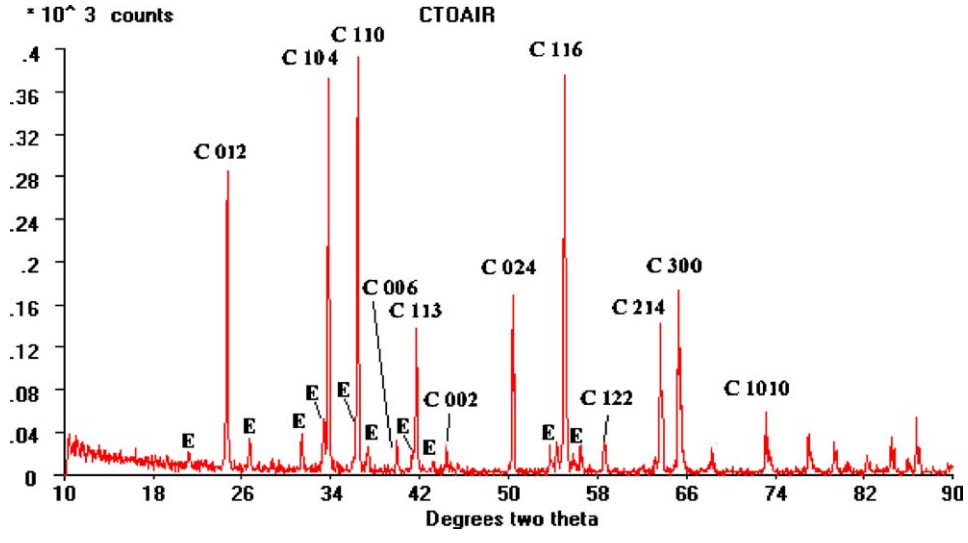

Figure 3 XRD plot obtained from air sintered $Cr_{1.8}Ti_{0.2}O_{3+x}$.

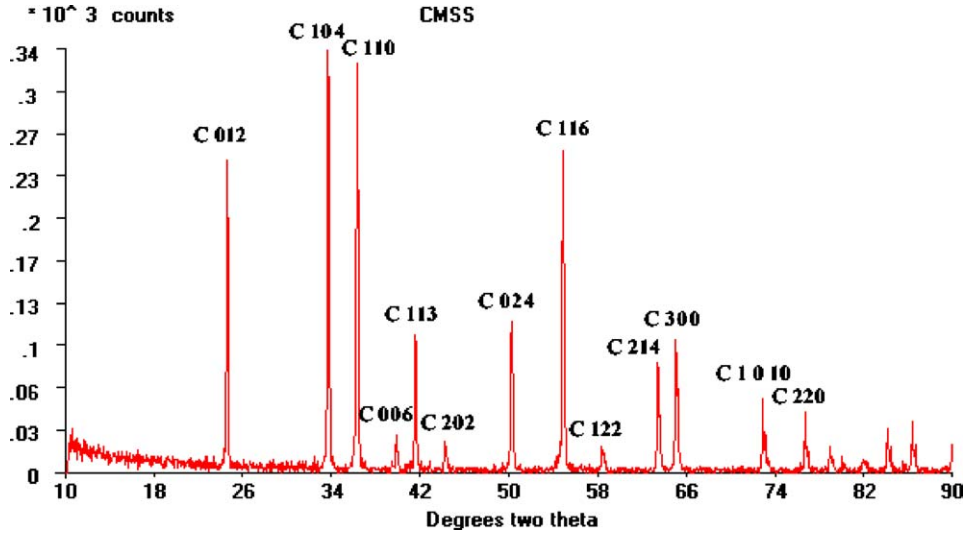

Figure 4 XRD plot obtained from reducing atmosphere sintered $Cr_{1.8}Ti_{0.2}O_{3+x}$.

reported above 1300°C, suggests that the E-phase is present in compositions of the mixed oxide from the chromia rich end down to a Cr/Ti metal atom% ratio of 25:75. i.e., Ti rich. The XRD plot in Fig. 3 shows assigned (hkl) values for the major peaks corresponding to α-Cr_2O_3 (prefixed by C) and peaks due to the formation of the E-phase denoted simply by E.

In comparison, Fig. 4 demonstrates that the diffraction data collected from reducing atmosphere sintered materials can be completely assigned to (hkl) values for undoped α-Cr_2O_3 and there is no apparent evidence of a second phase. On calculation of the relative intensities, the (116) peak in the Ti-doped single phase material was found to be 11% less intense than

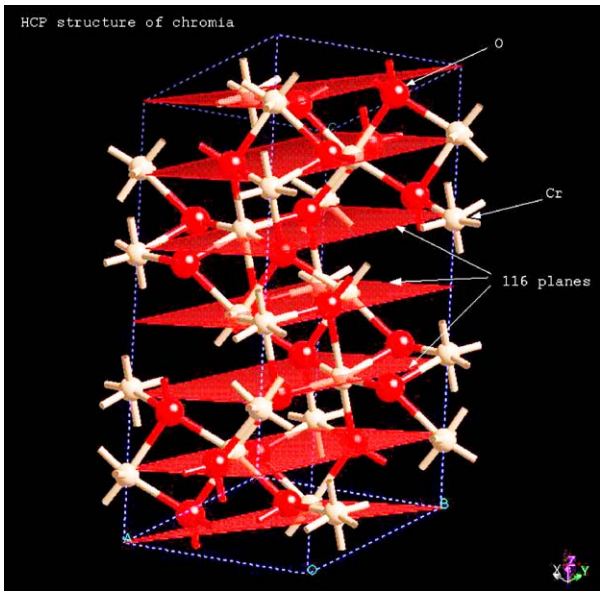

Figure 5 Crystal model highlighting (1 1 6) type planes in α-Cr_2O_3.

the same peak observed for pure α-Cr_2O_3. Crystallographic modelling of α-Cr_2O_3 using Cerius 2 MSI software, shows that the (1 1 6) family of crystallographic planes is host to the cations which are located in octahedral interstitials between closed packed anion layers as shown in Fig. 5. After a Nelson-Riley refinement of the data, corundum-type unit cell lattice parameters a and c for both α-Cr_2O_3 and $Cr_{1.8}Ti_{0.2}O_{3+x}$ were found to be identical within 4 significant figures, values of $a = 4.977 \pm 0.001$ and $c = 13.642 \pm 0.001$ Angstroms were extrapolated.

A selected area electron diffraction pattern obtained from a single grain of the reducing atmosphere mixed sintered material is displayed in Fig. 6 and shows that the substitution of Cr by Ti in α-Cr_2O_3 does not alter the structure or symmetry of the unit cell, the pattern has been indexed to the [1 0 $\bar{1}$ 0] zone axes following the electron diffraction study of α-Al_2O_3 by Lee and Lagerlof [16].

3.4. Chemical analysis, XPS and TEM/EELS

XPS allows a quantitative assessment of the elemental composition and chemical environment of species within the top few nanometres of the surface of a powder or densified pellet. XPS measurements made on the air-sintered material confirmed the presence of Ti^{4+} and Cr^{3+} with binding energies for Cr $2p_{3/2}$ and Ti $2p_{3/2}$ calculated to be 576.3 and 457.9 eV after charge correction. These values are in good agreement with the binding energies found in the native oxides; α-Cr_2O_3 and TiO_2 for which Cr $2p_{3/2}$ is 576 eV and Ti $2p_{3/2}$ is 458.8 eV. The curve fitting for both cation species described the measured curves well in terms of a single oxidation state, elemental quantification revealed that the composition of the surface region was significantly Ti-enriched over the expected target composition. After quantification, the surface Cr/Ti atom% ratio was determined to be 70:30 contrasting strongly with the target composition of 90:10.

For the material sintered under reducing atmospheres, the binding energies of Cr $2p_{3/2}$ and Ti $2p_{3/2}$ were found to be 576.9 and 458.7 eV respectively, again these are in good agreement with the values reported for the native oxides [17]. Curve fitting indicates the presence of a single oxidation state for both cations and importantly the surface composition was found to be almost identical to the target composition (Cr:Ti atom%) of 90:10, i.e., there was no surface enrichment of Ti. Material from both sintering regimes contained oxygen in the levels predicted by stoichiometry to within ± 1 atom%.

Representative HRTEM images, shown in Fig. 7, of crushed sintered samples dispersed on holey carbon covered copper grids suggested that the surface region of the air sintered material was structurally modified over the grain core structure. In comparison, images of the reducing atmosphere sintered material generally displayed continuous lattice fringes extending from the core of the grain to the surface without apparent disruption.

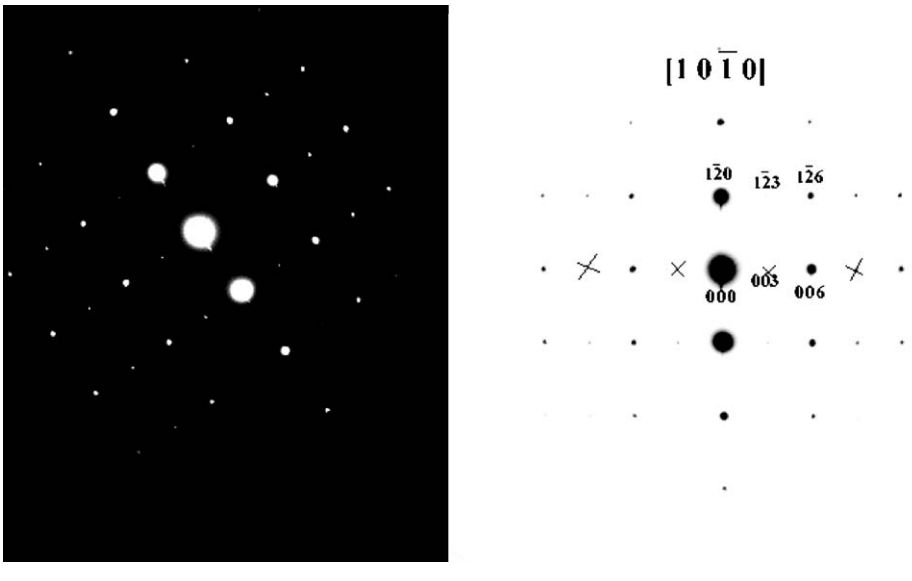

Figure 6 Diffraction pattern and indexed spots (rotated clockwise for clarity) for the [1 0 $\bar{1}$ 0] zone in $Cr_{1.8}Ti_{0.2}O_{3+x}$.

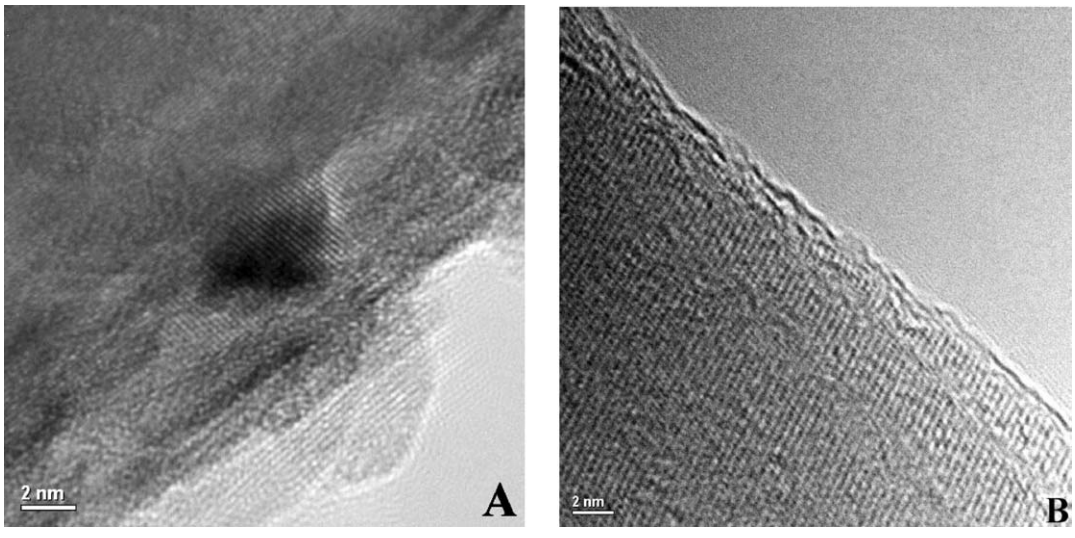

Figure 7 HREM images of air sintered material (A) and reducing atmosphere sintered material (B).

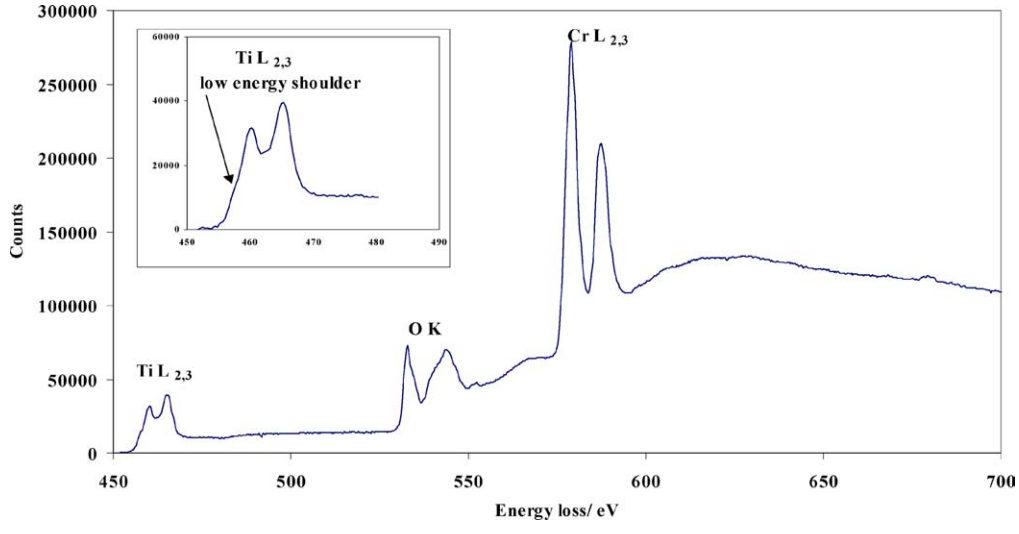

Figure 8 Background subtracted EELS spectrum from air sintered $Cr_{1.8}Ti_{0.2}O_{3+x}$ grain.

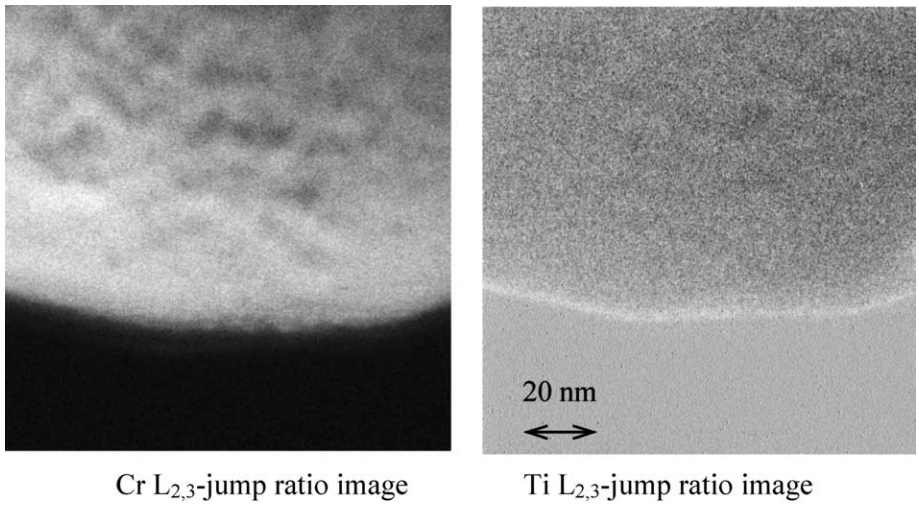

Figure 9 Energy filtered imaging of air sintered $Cr_{1.8}Ti_{0.2}O_3$ grain.

However, imaging surface modifications using HRTEM is somewhat contentious and consequently EELS microanalysis and EFTEM were also employed. Quantification of EELS spectra taken in diffraction mode (with a collection angle of 6 mrads) and collected from the interior core of powder particles revealed that they were Cr-rich; a typical spectrum being shown in Fig. 8, from which the Cr:Ti atomic ratio was quantified as being 95:5 atom%. The spectrum shows the position (peak maxima) of the Ti L_3-, Cr L_3 and O K edges at 458.6 eV, 579.0 eV at 533.0 eV respectively. By selecting relevant energy windows (of width 20 eV) positioned both prior to and at the Ti $L_{2,3}$- and Cr $L_{2,3}$ edges, energy filtered imaging (Fig. 9) of

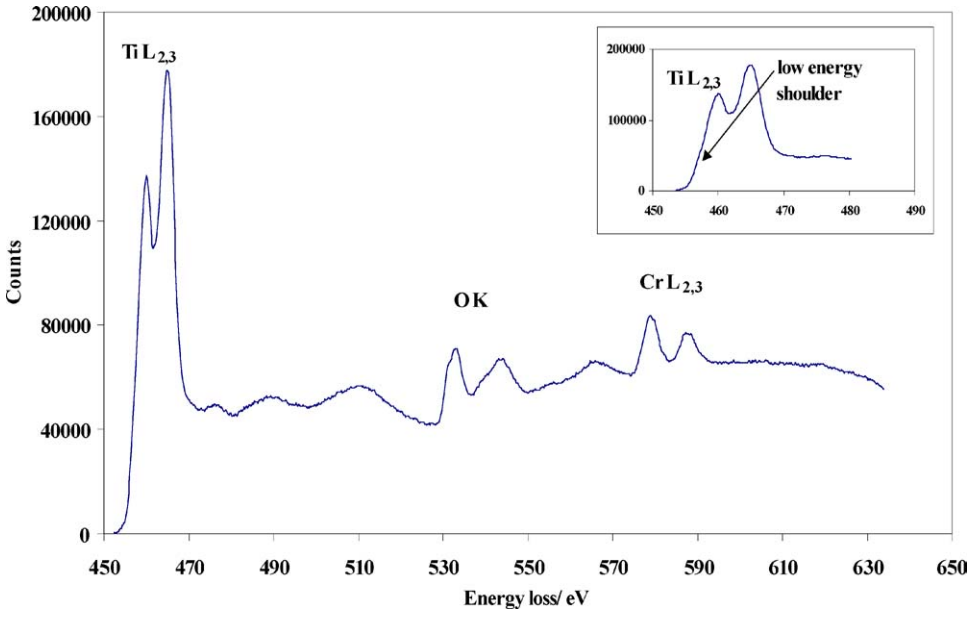

Figure 10 Background subtracted EELS spectrum from an air sintered $Cr_{1.8}Ti_{0.2}O_{3+x}$ particle surface.

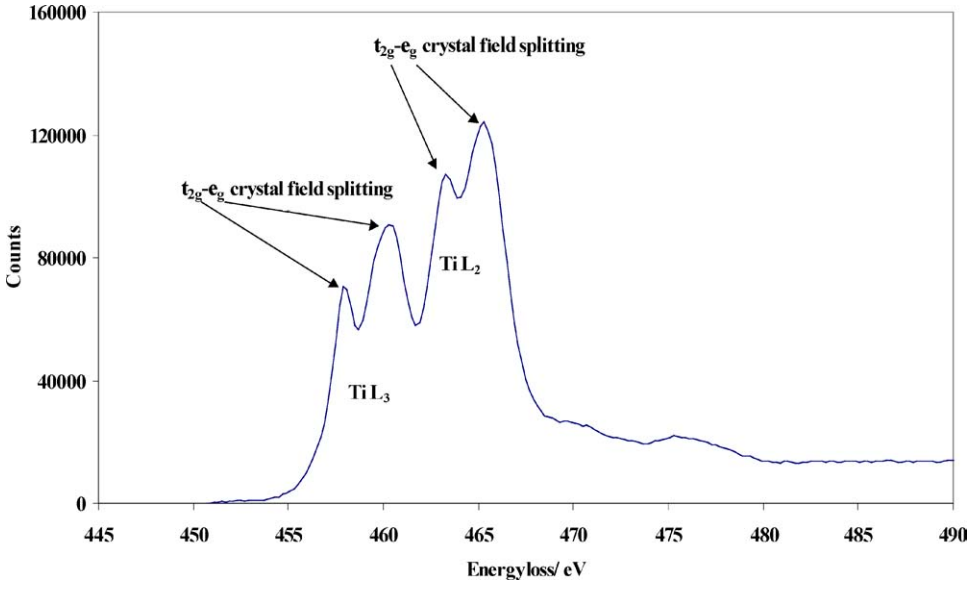

Figure 11 EELS Ti $L_{2,3}$-edge spectrum from the rutile polymorph of TiO_2.

grains revealed the elemental distribution of both elements within the microstructure down to a resolution of nanometres. Note that although jump-ratio images employed in this work are inherently non-quantitative, they do reveal clearly the distribution of elements within a microstructure with reduced effects from diffraction contrast. In Fig. 9, the white halo which can be seen at the edge of the particle in the Ti $L_{2,3}$ jump ratio image, indicates that the surface is enriched in Ti, conversely the absence of a sharp edge in the Cr $L_{2,3}$ jump ratio image implies that this region is Cr deficient. An EELS spectrum, taken in diffraction with a 100 nm SAED aperture mode, from the edge of this particle is shown in Fig. 10 and, in comparison with Fig. 8, it highlights the compositional variation between the particle bulk and surface. The edge positions of the spectra taken from the particle surface (Fig. 10) were identical to those given above for the bulk. Quantification of EELS spectra taken from the edge of this particle confirmed that the surface was Ti rich relative to the particle core, the Cr:Ti atom% ratio was measured to be ca. 30:70 atom%.

In addition to quantitative compositional information, EELS can also provide an insight into local atomic environments of component atomic species. In the spectra inset in Figs 8 and 10, closer inspection of the Ti L_3- and L_2-edges reveal two peaks due to the crystal field splitting of the 3d energy levels. This is a frequently observed phenomenon in metal oxides and is related to the chemical environment in which ions reside. The spectrum shown in Fig. 11 is that of the Ti $L_{2,3}$-edge as found in the rutile polymorph of TiO_2. Here the Ti L_3- and L_2-edges reveal two peaks of approximately equal intensity, arising from the octahedral coordination of Ti by O in rutile (in terms of crystal field theory, the t_{2g}-e_g peaks at 458 and 460 eV). The splitting observed in the chromia-titania spectra in Figs 8 (inset) and 10 (inset) is not so distinct and appears principally as a low

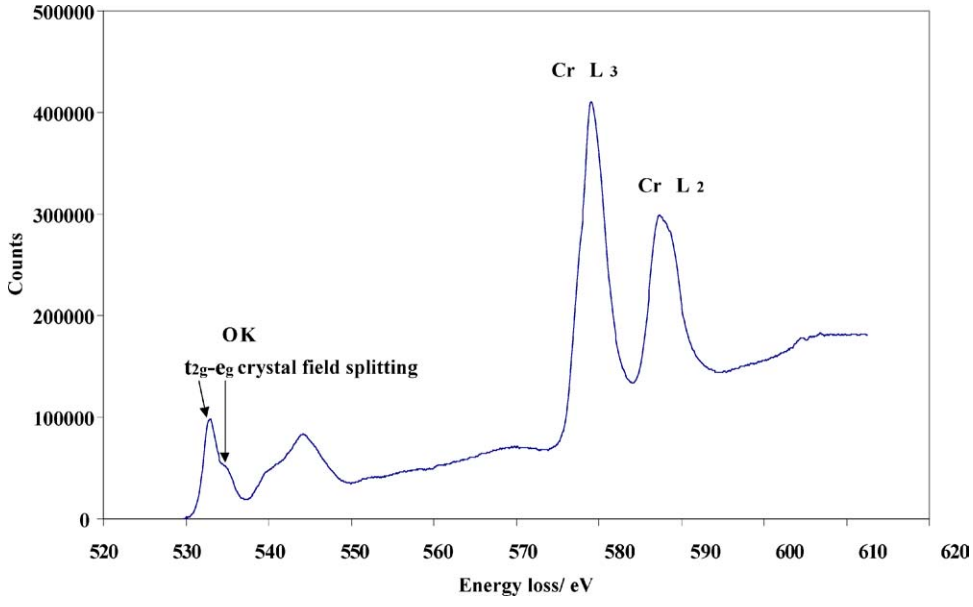

Figure 12 Background subtracted EELS spectrum from pure Cr_2O_3.

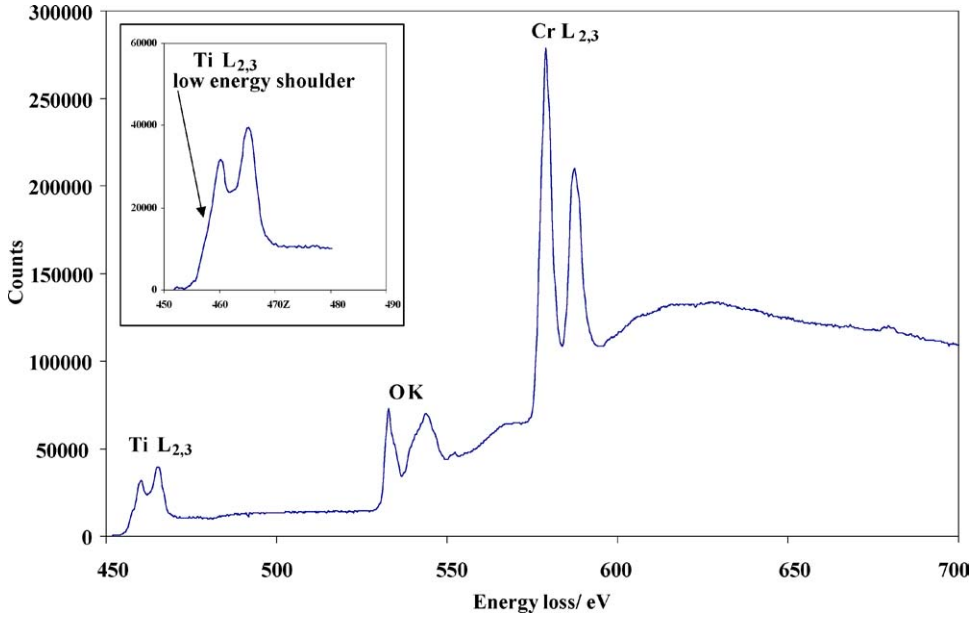

Figure 13 Background subtracted EELS spectrum from densified $Cr_{1.8}Ti_{0.2}O_{3+x}$ sintered under reducing atmosphere.

energy shoulder on each of the L_3- and L_2-edges. This would suggest that the Ti-rich phase found at the surface is not structurally the same as in TiO_2; suggesting that Ti may be incorporated into the Cr_2O_3 structure forming a discrete ternary phase contained solely at the surface. In the spectrum for rutile, the maximum of the first peak at the Ti L_3 edge appears at 458 eV, this value agrees well with the measured Ti L_3 edge in $BaTiO_3$ (Brydson *et al.*, 1993) [18] where Ti is also present as Ti^{4+}. The energy of the Ti L_3 peak in spectra obtained from the core and surface of the air sintered material, shown in Figs 8 and 10 is 458.6 and 458.8 eV respectively and would therefore also suggest Ti is present in both Cr-rich and Ti-rich surface regions as Ti^{4+}.

EELS spectra were also recorded from Cr_2O_3 to establish the O K- and Cr $L_{2,3}$- edge positions and shapes for the unmodified pure material. The EELS spectrum from Cr_2O_3 (Fig. 12) shows the position of the O K edge peak maximum at 533.0 eV and the Cr L_3 edge peak maximum at 579.0 eV. By comparing the shapes of the edges in Figs 10 and 8 with that in Fig. 12, it can be seen that there is there is no distinct difference in the Cr $L_{2,3}$- or O K- ELNES. This implies that the environment surrounding Cr and O has not been significantly altered in either the Ti-rich surface or Cr-rich bulk phases, i.e., the coordination number and symmetry is relatively unchanged. The edge positions and shapes in the spectra obtained for Cr_2O_3 are in excellent agreement with those obtained by Kurata *et al.* (1988) [19] who first reported the location of the Cr L_3-edge in Cr_2O_3 at 579.0 eV.

EELS spectra collected from the fully densified, reduced atmosphere sintered chromia-titania materials show that Cr $L_{2,3}$- and O K edges are almost identical to those exhibited in spectra obtained from pure Cr_2O_3. The spectrum shown in Fig. 13 was quantified to give a Cr:Ti atom% ratio of 90:10 atom% in good

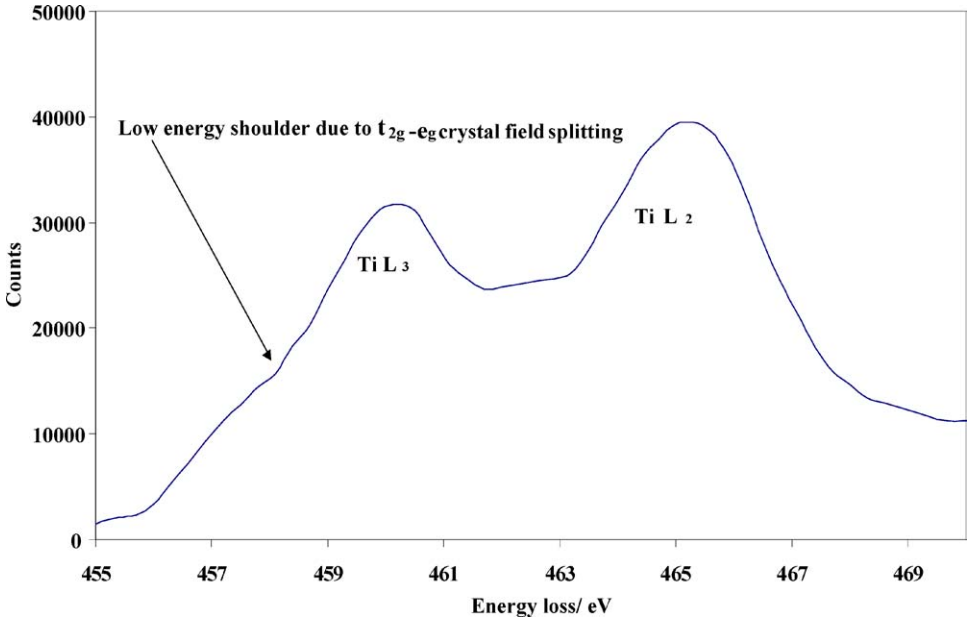

Figure 14 EELS spectrum of Ti $L_{2,3}$-edge in densified $Cr_{1.8}Ti_{0.2}O_{3+x}$ sintered under reducing atmosphere.

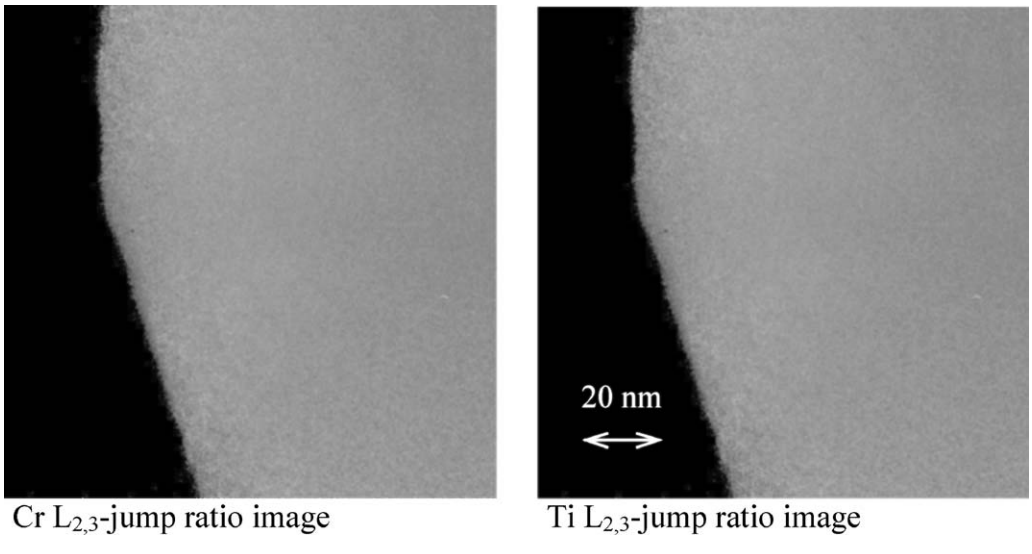

Figure 15 Energy filtered imaging of densified reducing atmosphere sintered $Cr_{1.8}Ti_{0.2}O_{3+x}$ particle.

agreement with the target composition. The Ti L_3-, O K- and Cr L_3-edges peak maxima are located at 459.9 eV, 533.0 and 579.0 eV respectively; the energy positions are in excellent agreement with the respective peaks measured in pure Cr_2O_3 and the rutile polymorph of TiO_2 (containing Ti^{4+}). The O K- and Cr $L_{2,3}$-edges do not show any significant difference in their shape when compared to those for pure Cr_2O_3, which suggests that the environment in which Cr and O reside has not been modified by the incorporation of Ti into a single homogeneous phase. The expanded spectrum shown in Fig. 14 shows a weak crystal field splitting of the Ti L_3 peak with a small low energy shoulder being apparent. As discussed earlier, the same peak in rutile exhibits a clear crystal field splitting and it is expected that the incorporation of Ti into the Cr_2O_3 cation sub-lattice would account for the reduced splitting observed. If Ti substitutes onto the Cr sites in Cr_2O_3 then the octahedral coordination of Ti by O is somewhat distorted compared to the octahedral coordination of Ti by O in rutile.

In the air sintered material surface enrichment of Ti was notable, however this was not observed in the densified material sintered under reducing conditions. This was confirmed by EFTEM imaging shown in Fig. 15. In the EFTEM jump ratio images, the distribution of Ti and Cr appears to be uniformly distributed between the particle surface and bulk. There is no evidence to support surface enrichment of Ti and corresponding spatially resolved EELS spectra suggested that no compositional variation existed between neighbouring particles. The Cr:Ti atom% ratio from a large number of specimen areas was consistently measured to be ca. 90:10 atom%: the target composition for this material.

4. Discussion

The reducing atmosphere employed to sinter titania-doped α-Cr_2O_3 materials was achieved by sealing pellets in Al_2O_3 crucibles with activated carbon included in order to create the low oxygen partial pressures required to densify green bodies. This method of sintering has

undoubtedly been successful in producing dense and homogenous ceramics, the highest density obtained using the enclosure was 5.08 g cm^{-3} (99.5% ρ_{th}). In contrast, Ownby [5] reported similar densities for undoped α-Cr_2O_3 achieved at a considerably higher temperature of 1600°C. At lower sintering temperatures employed in the present study, the densification of titania-doped chromia was still marked down to a maximum sintering temperature of 1250°C where sintered densities of 95% ρ_{th} were obtained.

The lower densities achieved from the sintering of undoped α-Cr_2O_3 suggests that the inclusion of TiO_2 in Cr_2O_3 is critical for enhancing the densification of the sesquioxide. Undoped α-Cr_2O_3 has been densified to 93.2% ρ_{th} at 1400°C for a dwell time of 4 h in the same enclosure. Below 1300°C, densification of the pure sesquioxide was not possible, even though the oxygen partial pressure predicted by equiTherm was low enough to suppress condensation-evaporation mechanisms. Under these conditions it is likely that the kinetic barrier to sintering could not be overcome and the temperature dependence of the mobility of diffusing species and the vacancy concentrations are limiting the final pellet densities that can be achieved.

EquiTherm calculations have predicted that during the optimum sintering regime (i.e., 1400°C for 4 h), the oxygen partial pressure may be as low as 6×10^{-14} atm. The densification of α-Cr_2O_3 is expected to be enhanced in atmospheres where the oxygen partial pressure is close to the Cr/Cr_2O_3 phase boundary. As stated earlier the oxygen partial pressure at this phase boundary has been calculated to be 5×10^{-15} atm at 1400°C, the atmosphere inside the crucible should therefore have been low enough to enhance densification of materials. However, the thermodynamic prediction of the oxygen partial pressure in the system may be an underestimate as it is anticipated that oxygen diffusion through the crucible will have occurred causing fluctuations, albeit temporary, in the oxygen content of the sealed system.

Sintering α-Cr_2O_3 and $Cr_{1.8}Ti_{0.2}O_{3+x}$ in laboratory air at 1400°C for 4 h produces no detectable change in pellet geometry from the green state, i.e., no densification occurs. From a microstructural point of view, the addition of Ti to α-Cr_2O_3 has little or no effect if air sintering is performed. $Cr_{1.8}Ti_{0.2}O_{3+x}$ material sintered in air displays considerable grain growth and a non-uniform distribution of Cr and Ti throughout a porous structure. Chemical analysis of this material has revealed the composition of most particles to be close to pure α-Cr_2O_3 with a surface segregation of Ti which forms a distinct surface phase. Surface diffusion of Ti over α-Cr_2O_3 particles would appear to be a significant event in the formation of the crystalline phases detected in air sintered CTO compositions. XRD measurements showed the presence of α-Cr_2O_3 and the E-phase (entirely consistent with the phase diagram after Werner, 1974 [15]), this evidence when combined with energy filtered TEM and XPS measurements, both of which revealed surface segregation of Ti, would suggest that the majority of air sintered particles display a core of α-Cr_2O_3 surrounded by an outer shell of E-phase.

The segregation of Ti to the surface of Cr_2O_3 particles has been predicted to arise as a result of a segregation driving force due to electrostatic charge effects [20]. The initial assumption that a true solid solution of Ti in Cr_2O_3 can form in air sintered materials implies that Ti diffuses, presumably via lattice diffusion through the bulk of α-Cr_2O_3 particles. The observed segregation of Ti to free surfaces and grain boundaries has then to be explained by electrostatic charge effects, as lattice strain effects because of cation size mismatches can be ruled out since the ionic radii of Ti^{4+} and Cr^{3+} only differ by 1 pm. This would appear unlikely as the results from the present work suggest that in air sintered materials, diffusion of Ti occurs only across surfaces where it reacts to form a ternary compound. It should be pointed out that if the predicted charge compensation of defects occurs, i.e., the substitution of three Cr^{3+} ions by three Ti^{4+} ions to create a Cr^{3+}vacancy, then charge neutrality prevails and surface segregation may not necessarily be favourable in terms of electrostatic charge considerations. In short, it would seem that air sintered $Cr_{1.8}Ti_{0.2}O_{3+x}$ materials do not display a true solid solution after sintering at 1400°C, instead they form a 2 phase system, consisting of α-Cr_2O_3 and E-phase.

Examination of reducing atmosphere sintered $Cr_{1.8}Ti_{0.2}O_{3+x}$ materials revealed that they were a true solid solution exhibiting no surface enrichment or segregation of Ti. A combination of XPS and EELS has revealed that the surface composition of these oxides is identical to the bulk and that the chemical distribution of Ti and Cr, is uniform throughout sintered pellets. XRD measurements have also provided strong evidence for the formation of a true single phase solid solution identical in structure to α-Cr_2O_3, the lattice parameters have been determined and show no change on the substitution of Cr^{3+} by Ti^{4+}. Peak intensity variations have been observed in particularly for the (1 1 6) peak and Fig. 5 shows the {1 1 6} set of planes in α-Cr_2O_3 drawn to highlight their cation occupancy. Assuming that Ti^{4+} substitutes for Cr^{3+} on the same octahedral sites, one can see that the {1 1 6} set of planes is host to cations as indicated. It would follow that the substitution of Ti^{4+} on Cr^{3+} sites would alter the intensity with which incident X-rays are scattered, i.e., the atomic scattering factors are different. The atomic scattering factor is dependent on the X-ray scattering angle and related to the number of electrons associated with an atom/ion as these are principally the diffracting objects. The (116) plane resides at a $\sin\theta$ value of approximately 0.46, at which the atomic scattering factors for Ti^{4+} and Cr^{3+} are 9.10 and 10.22 respectively [21]. The lower relative intensity of this peak in Ti doped α-Cr_2O_3 compared to that seen in pure α-Cr_2O_3 is therefore consistent with the proposed structural model for the solid solution phase.

EELS spectra collected from $Cr_{1.8}Ti_{0.2}O_{3+x}$ materials have revealed differences in the shape of the Ti $L_{2,3}$ edge with respect to the edge obtained in TiO_2. The crystal field splitting seen in TiO_2 arises from the coordination of Ti by oxygen in the form of TiO_6 octahedra. The transition metal 3d-orbitals consist of several

components of differing spatial directionality, some of the components of the 3d-orbitals point directly at the coordinating atoms whilst others are at an angle to the bonding direction. The resulting crystal field splits the unoccupied portion of the transition metal 3d band into low and high energy components termed the t_{2g} and e_g molecular orbitals or bands. If the symmetry of the oxygen ligands surrounding the Ti^{4+} ion is altered from perfect octahedral then the resulting crystal field splitting is also modified. For the case of Ti substitution on a Cr site in α-Cr_2O_3, the site can be considered to be of a lower symmetry than D_{4h} as found in rutile and the crystal field splitting is reduced as the direction of the bonding orbitals is rotated. The MO_6 octahedron (where M is a transition metal) is clearly distorted in α-Cr_2O_3, if Ti resides at this site then the crystal field splitting would be expected to be diminished. Low energy shoulders (probably due to a diffuse t_{2g} state caused by changes in bond angle and/or bond lengths) are visible on the Ti L_3-edge for chromia-titania materials (both air sintered and reducing atmosphere sintered) suggesting that the TiO_6 coordination symmetry is not the same as in TiO_2. It is reasonable to expect that this effect will also occur in the E-phase residing at the surface of air sintered materials, however, very little is known about the exact structure of this phase and so no firm conclusion can be drawn concerning the coordination and symmetry of cations by oxygen.

Both the energy positions of the Ti $L_{2,3}$- and Cr $L_{2,3}$-peaks determined by EELS, and the Ti $2p_{3/2}$ and Cr $2p_{3/2}$ peak energies measured by XPS, confirmed the presence of Ti as Ti^{4+} and Cr as Cr^{3+} in all materials. It was notable that the oxidation state of Ti could be misinterpreted as being a mixture of more than one oxidation state if ion beam sputter-cleaning was performed on samples prior to measurement by XPS.

Based on the present results, the following mechanism is tentatively proposed to account for the role of Ti in the sintering of α-Cr_2O_3 under reduced oxygen partial pressures:

- At oxygen partial pressures close to the Cr/Cr_2O_3 phase boundary (i.e., reducing conditions), the oxygen vacancy concentration is significantly increased over that seen in normal atmospheres. If the diffusion of oxygen is the rate controlling mass transport step in the normally highly stoichiometric chromia lattice, the introduction of oxygen vacancies increases the anion diffusivity and as a result the densification is enhanced.
- The creation of oxygen vacancies and partial opening of surrounding oxygen cages also allows and enhances the diffusion and movement of Cr^{3+} ions out of their original octahedral sites causing less lattice strain energy. The vacation of such sites then allows ingress of Ti^{4+}, which can then occupy regular Cr^{3+} lattice sites thus creating a substitutional solid solution.
- At low oxygen partial pressures, the chromium vacancy concentration is very low and chromium interstitials are the dominant point defects. The introduction of Ti^{4+} requires the formation of chromium vacancies for charge neutrality to prevail. In polycrystalline α-Cr_2O_3, the diffusivity of Cr^{3+} is high due to pipe diffusion along grain boundaries, in single crystals however, cation diffusion is rate limiting in growth processes, presumably due to inherently low cation lattice diffusion. This is supported by Crystal Field Preference Energy (CPFE) considerations [22] which suggest that the mobility of Cr^{3+} through the oxide is exceptionally low. The chromium vacancies introduced by doping α-Cr_2O_3 with Ti^{4+}, enhance lattice diffusion of Cr^{3+} so aiding densification and also opening a path for the further ingress of Ti^{4+} through the α-Cr_2O_3 lattice so as to create a true single phase solid solution.
- The volatile higher oxides of Cr are prevented from forming at low oxygen partial pressures, therefore inhibiting grain growth phenomena and maintaining the driving force for densification.

Drawing a comparison to air sintered $Cr_{1.8}Ti_{0.2}O_{3+x}$ materials where no true solid solution is observed, one can speculate that the inherently low oxygen vacancy concentration in normal atmospheres controls the densification behaviour. In addition, it would seem reasonable that the oxygen population partly controls the movement of Cr^{3+} via bulk or lattice diffusion paths making ingress of Ti through the lattice difficult and therefore preventing the formation of a solid solution. The difficulty with which solid solutions of Ti form in α-Cr_2O_3 is reflected in the α-Al_2O_3-TiO_2 system (Li *et al.*, 1999) [23] where the surface compositions of α-Al_2O_3 particles is found to be almost pure rutile. The inert character of these corundum structures may be a key feature in explaining why it is so difficult to form mixed metal compounds where the host material is the sesquioxide.

5. Conclusion

It has been shown that it is possible to densify $Cr_{1.8}Ti_{0.2}O_{3+x}$ to near theoretical densities using an inexpensive sample enclosure, in which the oxygen partial pressure is controlled by the presence of activated carbon. Reducing atmosphere sintered $Cr_{1.8}Ti_{0.2}O_{3+x}$ material sinters to almost theoretical density (ρ_{th}). The temperature at which densities in excess of 99% ρ_{th} can be achieved are at least 200°C lower than for the sintering of pure α-Cr_2O_3. There remains a striking dependence of the densification of these materials on the oxygen partial pressure and this study has revealed that it is the conditions under which densification can be achieved that allow the formation of a single phase and therefore a true solid solution. This material shows a uniform distribution of both Ti and Cr throughout the micro and nano-structure and XRD, EELS and XPS have all confirmed the substitution of Ti onto regular Cr lattice sites as Ti^{4+} causing negligible lattice distortion. In contrast air sintered material exhibits a distinct surface enrichment of a chromia-titania ternary phase (E-phase) on the surface of chromia cores. We hope that this study has highlighted the powerful combination of analytical TEM, diffraction and surface analytical

techniques for the determination of chemical and microstructural development in complex ceramic systems as a function of processing conditions.

Acknowledgements

SPM gratefully acknowledges and EPSRC studentship together with financial support from an industrial sponsor.

References

1. G. S. HENSHAW, D. H. DAWSON and D. E. WILLIAMS, *J. Mater. Chem.* **5**(11) (1995) 1791.
2. P. T. MOSELEY, J. O. W. NORRIS and D. E. WILLIAMS (eds.), in "Techniques and Mechanisms in Gas Sensing" (Adam Hilger, Bristol, 1991).
3. K. NAGAI and K. OBHAYASHI, *J. Amer. Ceram. Soc.* **72**(3) (1989) 400.
4. W. D. CALLISTER, M. L. JOHNSON, I. B. CUTLER and R. W. URE, *ibid.* **62**(3/4) (1979) 208.
5. P. D. OWNBY, "Materials Science Research Vol. 6: Sintering and Related Phenomena" edited by Kuczynski (Plenum Press, NY, 1972) p. 431.
6. S. N. ROY, S. R. SAHA and S. K. GUHA, *J. Mater. Sci*. **21** (1986) 3673.
7. D. H. DAWSON, G. S. HENSHAW and D. E. WILLIAMS, *Sens. and Actuat.* B **26/27** (1995) 76.
8. P. W. ATKINS, "Physical Chemistry"(Oxford University Press, Oxford, 1994) p. C25.
9. R. BRYDSON, "Electron Energy Loss Spectroscopy" (Bios, Oxford, 2001).
10. C. HAMMOND, "The Basics of Crystallography and Diffraction," 2nd ed. (OUP, Oxford, 2001).
11. J. F. WATTS and J. WOLSTENHOLME, "Introduction to Surface Analysis by XPS and AES" (Wiley, Chichester UK, 2003).
12. P. D. OWNBY and G. E. JUNGQUIST, *J. Amer. Ceram. Soc*. **55**(9) (1972) 433.
13. T. CHOUDHURY, S. O. SAIED, J. L. SULLIVAN and A. M. ABBOT, *J. Phys. D: Appl. Phys*. **22** (1989) 1185.
14. M. HAMELIN, *Bull. Soc. Chim., France* (1957) 1421.
15. H. D. WERNER, *Neus. Jahrb. Miner. Montash*. H5 (1974) 218.
16. W. E. LEE and K. P. D LAGERLOF, *J. Electron Microsc. Techn.* **2** (1985) 247.
17. J. F. MOULDER, W. F. STICKLE, P. E. SOBOL and K. D. BOMBEN, "Handbook of X-ray Photoelectron Spectroscopy" edited by J. Chastain, R. C. King (Physical Electronics Ltd., Minnesota, USA, 1995).
18. R. BRYDSON, L. A. J. GARVIE, A. J. CRAVEN, H. SAUER, F. HOFER and G. CRESSEY, *J. Phys: Condens. Matter*, **5** (1993) 9379.
19. H. KURATA, K. ISHIZUKA and T. KOBAYASHI, *Bull. Inst. Chem. Res.* **66** (1988) 572.
20. D. NIEMEYER, D. E. WILLIAMS, P. SMITH, K. F. E. PRATT, B. SLATER, C. R. A. CATLOW and A. M. STONEHAM, *J. Mater. Chem* **12**(3) (2002) 667.
21. C. H. MACGILLAVARY and G. D. RIECK (eds.), "International Tables for X-ray Crystallography" Vol. 3 (The United Union of Crystallography, Kynoch Press, 1962).
22. P. A. COX, "The Electronic Structure and Chemistry of Solids" (Oxford Science Publications, 1991) p. 236.
23. C. LI, J. HAN, Z. ZHANG and H. GU, *J. Amer. Ceram. Soc.* **82**(8) (1999) 2044.

Received 31 July 2003
and accepted 20 January 2004